ORNL/TM-2024/3439

Mini-99 Experiment Design and Target Assembly

Zane Wallen
Richard Howard
Kara Godsey
Annabelle Le Coq
Caleb Massey

June 2024

OAK RIDGE National Laboratory

ORNL IS MANAGED BY UT-BATTELLE LLC FOR THE US DEPARTMENT OF ENERGY

ORNL/TM-2024/3439

Nuclear Energy and Fuel Cycle Division

MINI-99 EXPERIMENT DESIGN AND TARGET ASSEMBLY

Zane Wallen
Richard Howard
Kara Godsey
Annabelle Le Coq
Caleb Massey

June 2024

Prepared by
OAK RIDGE NATIONAL LABORATORY
Oak Ridge, TN 37831
managed by
UT-BATTELLE LLC
for the
US DEPARTMENT OF ENERGY
under contract DE-AC05-00OR22725

Contents

LIST OF FIGURES

LIST OF TABLES

ABBREVIATIONS

ANL	Argonne National Laboratory
APDL	Ansys Parametric Design Language
BOC	beginning of cycle
DAC	design and analysis calculations
DOE	US Department of Energy
EABD	experiment authorization bases document
EB	electron beam
EOC	end of cycle
HEU	highly enriched uranium
HFIR	High Flux Isotope Reactor
IEG	Irradiation Engineering Group
ISVXF	Inner Small Vertical Experiment Facilities
LCS	limiting condition scenario
LEU	low enriched uranium
LSM	lab space manager
MBA	material balance areas
MBAR	material balance area representative
MCNP	Monte Carlo N-particle
Mo-100	molybdenum-100
Mo-99	molybdenum-99
NDE	nondestructive examination
NEFCD	Nuclear Energy and Fuel Cycle Division
NMC&A	nuclear material control and accountability
NNSA	National Nuclear Security Administration
NRU	National Research Universal
OD	outside diameter
ORNL	Oak Ridge National Laboratory
PIE	post-irradiation examination
QA	quality assurance
RAS	Radial Axial Subassembly
RB*	Large Removeable Beryllium Facilities
SCALE	Standardized Computer Analyses for Licensing Evaluation
Tc-99m	technetium-99 (metastable)
TIG	tungsten inert gas
U-foil	uranium foil
Y-12	Y-12 National Security Complex

ACKNOWLEDGMENTS

This work was completed under the DOE National Nuclear Security Administration's Material Management and Minimization program in collaboration with Eden Pharmaceuticals.

The project was managed by Jim Nash and Jorge Navarro of ORNL.

The assembly of the target was made possible through the technical support of David Bryant of the ORNL Irradiation Engineering group and Breanna Vestal of the ORNL Fuel Cycle Chemical Technology group. Ryan Gallagher must also be acknowledged for his documentation and preliminary thermal analyses contributions in the early stages of this experiment prior to his departure from ORNL.

ABSTRACT

Qualification of nuclear fuels requires an understanding of a myriad of fuel performance characteristics, which requires time-consuming irradiations in test reactors. Accelerating burnup accumulation to reduce the irradiation time has historically been accomplished by increasing the ^{235}U enrichment in integral fuel tests, which inherently couples the fuel's temperature and fission heat generation. Separate effects irradiation testing of nuclear fuel, using the MiniFuel target in the Oak Ridge National Laboratory's High Flux Isotope Reactor, offers an approach for decoupling fuel temperature and fission rate by reducing the quantity of the fuel and relying primarily on gamma heating in the surrounding components to drive fuel temperatures; however, if the fission rate is high enough, the fuel temperature will still vary over time as the fission heating changes, primarily due to poor heat conduction between the fuel and the surrounding components. This work details the design, analysis, and fabrication of a MiniFuel target that utilizes sodium bonding to improve the heat rejection from the fuel specimen, enabling the testing of higher ^{235}U enrichments (~8 wt %) to further accelerate burnup accumulation without causing prohibitively large temperature variations throughout the course of the irradiation.

1. INTRODUCTION

Approximately 80% of medical diagnostic imaging utilizes the isotope technetium-99m (Tc-99m). Tc-99m has a half-life of just 6 hrs and is a decay product of molybdenum-99 (Mo-99), which itself has a half-life of only 2.7 days. Due to these short half-lives, Mo-99 and Tc-99m must be regularly and consistently produced and/or acquired; however, almost all Mo-99 produced for this purpose is supplied by a select few international research reactors, several of which are approaching the end of their operating lives [1]. These reactors produce Mo-99 through the irradiation of highly enriched uranium (HEU), during which approximately 6% of fissions result in the production of the Mo-99 atom; however, due to increasing concerns about proliferation risks, all major producers now use low enriched uranium (LEU) [2]. Advanced Mo-99 production methodologies are under development, such as the irradiation of molybdenum-98 to induce neutron capture (n,γ reaction) to Mo-99 or the use of particle accelerators to bombard molybdenum-100 (Mo-100) with electrons (β,γ reaction) or protons (p,n or p,pn reaction), resulting in transmutation to Mo-99; however these methodologies are either performed on a small scale or are still under development.

Nearly the entire US supply of Mo-99 has been provided by research reactors outside the United States, primarily the National Research Universal (NRU) reactor in Canada, which is no longer operational, and the High Flux Reactor in the Netherlands. This has exposed the United States to risks in Mo-99/Tc-99m availability and price fluctuation when unexpected supply chain disruptions have occurred from these suppliers. To reduce US reliance on imported Mo-99, significant effort has been made to expand the domestic Mo-99 production capabilities by using conventional methodologies and existing infrastructure and to investigate advanced methodologies.

The specific activity of Mo-99 produced during irradiation can be increased substantially by utilizing a fuel form that maximizes the concentration of uranium. One of the advanced production capabilities is the use of high-density uranium foils (U-foils) as an alternative the standard U-aluminide or silicide variants as irradiation targets to produce Mo-99. This capability was previously investigated through a collaboration between Oak Ridge National Laboratory (ORNL), the Y-12 National Security Complex (Y-12), Argonne National Laboratory (ANL), and the University of Missouri. The research was made possible through funding by the US Department of Energy (DOE) National Nuclear Security Administration's (NNSA's) Office of Global Threat Reduction. This project oversaw the development of U-foil production and processing capabilities at Y-12, the irradiation of the U-foil targets at ORNL's High Flux Isotope Reactor (HFIR), and the post-irradiation chemical processing routes at ANL. (The project concluded in 2016.) The capabilities established during the investigation have been instrumental to the success of the experiments detailed in this report.

The primary objectives of this experiments were (1) to ascertain new knowledge about the competition between irradiation growth and swelling in Mo-99 production-relevant temperature regimes during irradiation of U-foil and (2) to create a database of high-density U-foil post-irradiation examination (PIE) data for companies to leverage during their future licensing efforts.

1.1 IRRADIATION OF HIGH-DENSITY U-FOIL

This work went a built on the previously established irradiation campaign for U-foil targets in an effort to track the irradiation response of the foils over the course of the target's lifetime. When uranium is irradiated, the material can give different microscopic and macroscopic responses as a function of prior thermomechanical processing history (i.e., texture development during fabrication), irradiation dose/dose rate, and irradiation temperature. During the initial development of metallic fuels for fast reactors in the 1950s and 60s, significant effort was put into understanding the irradiation response of uranium metal to

doses similar to those expected during the U-foil irradiations in this study. Consequently, this experiment provides a unique opportunity to compare the irradiation response of thin foils to larger tube or rod forms that have been previously irradiated in a variety of test reactors.

At lower irradiation temperatures, dislocation loops preferentially form on certain planes in the orthorhombic U lattice, which is the primary mechanism for anisotropic growth of uranium at temperatures up to 200°C to 300°C [3, 4, 5, 6]. This irradiation growth phenomenon at lower irradiation temperatures is the driving force for irradiation creep in alpha uranium [7]. The buildup of defects within the microstructure (interstitial-vacancy pairs, dislocation loops, etc.) and generation of new fission products change the physical and mechanical properties. Thermophysical properties (e.g., thermal conductivity) are important to target designers verifying that safe operating temperature limits are not being surpassed. At higher irradiation temperatures, vacancies generated within the lattice during irradiation begin to easily migrate and can form voids that grow and cause volumetric swelling within the material, which lowers the density of the alloy and increases the macroscopic volume. The cavities are stabilized by the buildup of gaseous fission products (such as xenon), which promotes their growth and exacerbates this phenomenon [8, 9, 10].

There may be an optimal irradiation temperature for the U-foil target irradiations that is between the two regimes and in which both defect mechanisms are minimized. For this reason, three irradiation temperatures were initially selected to span the growth and swelling temperature regimes to capture those effects. Although these target temperatures were later slightly altered (as discussed in Section 2.5), Figure 1 displays (1) a summary of historic data on U-foil growth and volumetric swelling rates as a function of irradiation temperature and (2) the original target temperature regimes selected at the conception of this experiment.

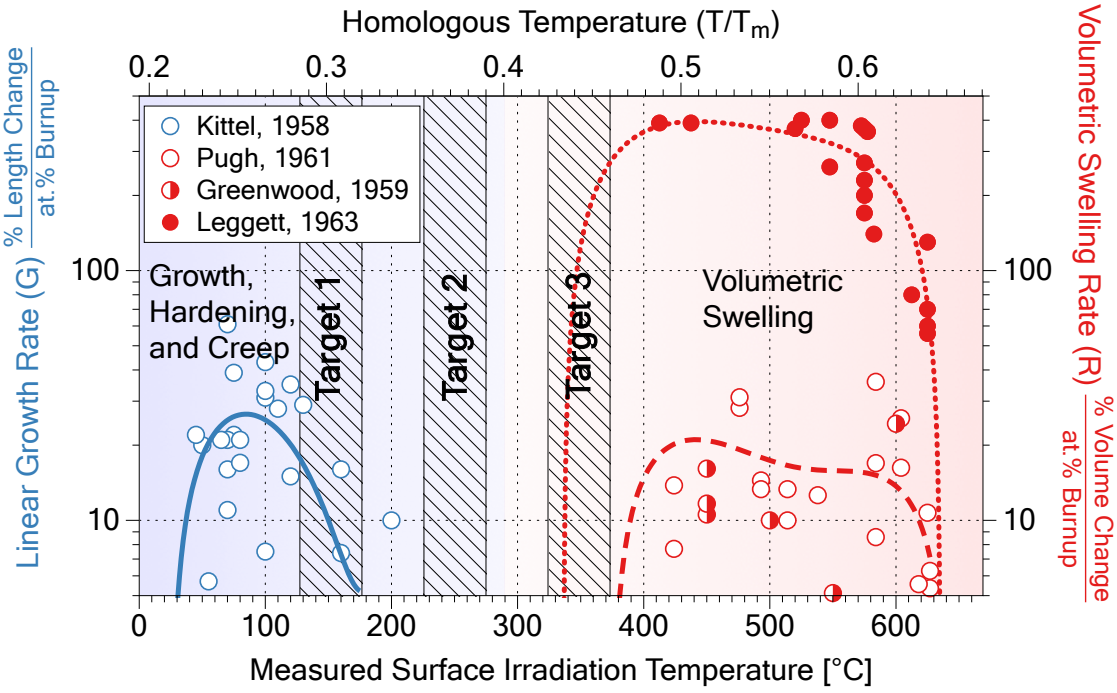

Figure 1. U-foil irradiation growth and volumetric swelling [4, 8, 9, 10].

1.2 ORNL CAPABILITIES IMPROVEMENT

The secondary goal of this experiment is to improve qualification capabilities for novel fuel concepts. The miniature fuel (MiniFuel) irradiation vehicle developed at ORNL was designed to perform separate effects irradiation testing of nuclear fuels in which fuel performance variables and fuel phenomena of interest are isolated [11]. Accelerating fuel burnup accumulation expedites the qualification of nuclear fuels by reducing the irradiation time. This has been accomplished by increasing the ^{235}U enrichment in integral fuel tests, which inherently couple the fuel's temperature and fission heat generation, which varies spatially and temporally. MiniFuel experiments have been used to decouple the fuel temperature and fission rate; the reduced fuel specimen size allows the gamma heating in the surrounding components to drive fuel temperatures. There are limits to this process of increasing the fuel enrichment and decreasing its size, however. Post-irradiation validation becomes increasingly difficult and unreliable as the fuel specimen size decreases, and, if the fission rate is high enough, the fuel temperature will still vary spatially and over time as the fission heating changes, primarily due to poor heat conduction between the fuel and the surrounding components. The utilization of liquid sodium bonding between the fuel and surrounding components improves the heat rejection from the fuel specimen, thus enabling the testing of higher ^{235}U enrichments (8 wt %) to further accelerate burnup accumulation and greatly reducing temperature variations.

2. EXPERIMENT DESIGN AND ANALYSIS

2.1 HFIR AND THE MINIFUEL VEHICLE

The HFIR is a pressurized light water–cooled and moderated flux-trap type reactor [12]. The core comprises highly enriched ^{235}U fuel in aluminum clad, involute fuel plates arranged into two concentric annuli and surrounded by removable and permanent beryllium reflectors, which also feature multiple positions for irradiation experiments, including the inner small vertical experiment facility (ISVXF) positions. Experiments are cooled by the moderator, which is between 50°C and 60°C [13]. MiniFuel experiments can be inserted into the ISVXF or the large removeable beryllium facility (RB*) positions within the HFIR [11, 14], which are highlighted in Figure 1.

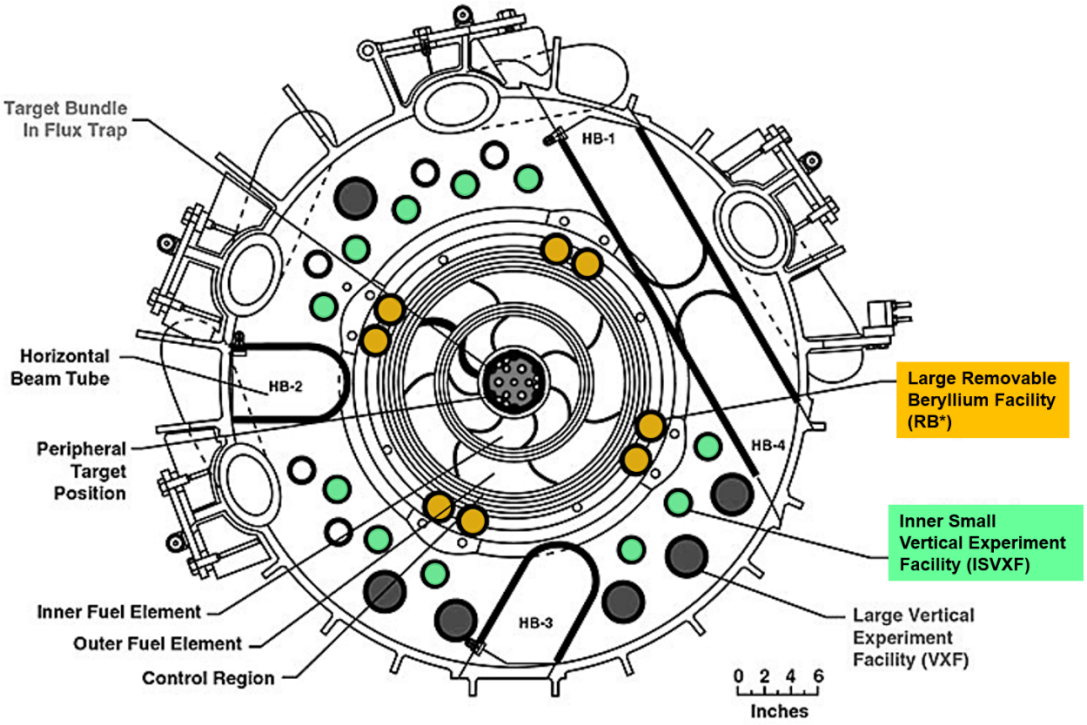

Figure 2. Top-down cross section of the ORNL HFIR core layout [15].

2.2 EXPERIMENT DESIGN

The experiments detailed in this report utilize the MiniFuel irradiation vehicle inserted into one of the ISVXF positions in an aluminum experiment basket. The experiment basket has three radial positions: two front positions equidistant from the core and one in a back position further away from the core. Each radial position contains three axial target positions. Therefore, each ISVXF MiniFuel basket can hold a total of nine experiment targets, each of which containing six subcapsules (also called subassemblies), allowing for a total of 54 MiniFuel subcapsules to be irradiated simultaneously in a single ISVXF. The Radial Axial Subassembly (RAS) nomenclature system, developed by members of the ORNL Nuclear Energy and Fuel Cycle Division (NEFCD), is used to identify the position of the subcapsules. The notation increases clockwise for the radial positions and upward for axial and subassembly positions. The

first position for the radial notation (position 1) is the back position (furthest from the core) and is the bottom position for the axial and subassembly.

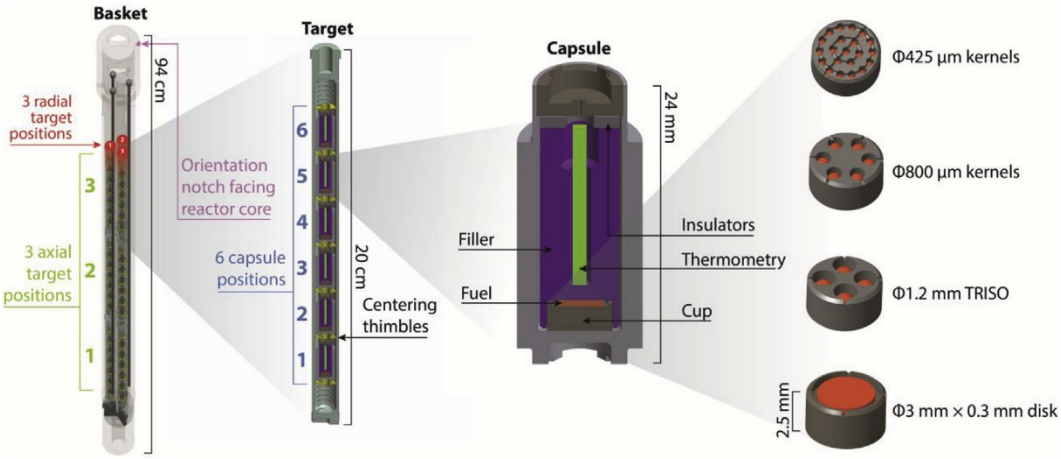

Figure 3. Experiment positions for the ISVXF basket [11].

Each target consists of the target housing, which comprises an outer tube, a bottom end cap, and a top end cap, six subcapsules, centering thimbles between each subcapsule, and stainless-steel springs at the top and bottom of the subcapsule stack. The components of the subcapsules are similar in design to those used in previous MiniFuel experiments [11, 14]. They feature a molybdenum holder of variable outer diameter, an end cap, Grafoil spacers, a SiC thermometry rod, a molybdenum tube, a fuel dish, and a fuel specimen. Where this experiment stands apart from previous MiniFuel experiments is the addition of a liquid sodium filler around the fuel, fuel dish, and bottom of the tube. Another unique feature is the fuel form and geometry, which is 8% enriched (by weight) uranium metal in disk form with nominal dimensions of 3.0 mm outer diameter and 0.4 mm thickness. (See Figure 4)

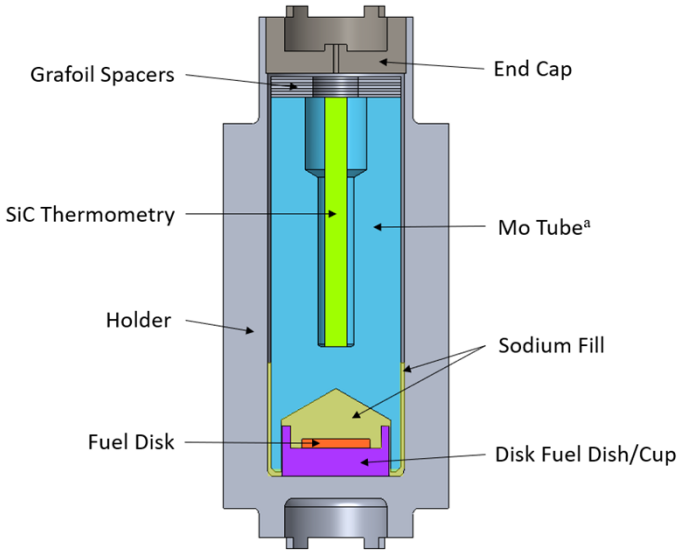

[a] The molybdenum tube features a small relief hole (not shown) that extends from above the fuel disk to the outer wall to allow any gas trapped above the fuel and dish to escape during assembly

Figure 4. CAD rendering of subcapsule components

The annular rim of the end cap is welded to the holder using an electron beam (EB) trepan weld. Tungsten inert gas (TIG) welding is used to manually weld the seal weld button shut after the subcapsule is backfilled with an inert gas. Centering thimbles are placed at each end of the subcapsule,which is thenstacked into a target housing. The target housing bottom and top end caps are EB-welded to the outer tube, and a fill hole in the top end cap is sealed by a TIG weld following target backfill with an inert gas.

2.3 NEUTRONICS ANALYSIS

Neutronic calculations were performed with representative target geometries and materials to determine the rates of fuel burnup and material heat generation (prompt neutron, prompt gamma, and local alpha/beta decay heat) as a function of time and position. The simulations were carried out using the HFIRCON Version 1.0.5, an ORNL developed code package that automates the workflow for high-fidelity, multicycle target depletion analysis in HFIR [16]. The package uses Python scripts and C plugins to integrate the data transfer between several programs, namely MCNP transport simulations and the SCALE ORIGEN depletion and decay calculations. HFIRCON code has been widely applied to various irradiation targets and previous MiniFuel experiments [14].

2.3.1 Target Geometry

The template model used for the calculation was a modified version of the cycle 400 beginning of cycle (BOC) MCNP HFIR model [17]. The previous modifications to the model were overwritten by the modifications for this model. The geometry for the target was manually created based on the engineering drawings of the experiment. (See Figure 6.) There are some geometric inconsistencies because the drawings are simplified and not final.

The target experiment was modeled within VXF-15, which has the highest thermal neutron flux of all the ISVXF positions [18], of the base HFIR model. VXF-15 is representative of all ISVXF positions, due to the radially symmetric design of HFIR. Figure 5 displays a cross section of the HFIR model with the target experiment present in VXF-15 and a zoomed-in view of the VXF experiment basket showing the orientation and radial position designations of the targets.

The geometry for the target was manually created based on drafts of the engineering drawings of the experiment. Figure 6 displays the model geometry for a subcapsule.

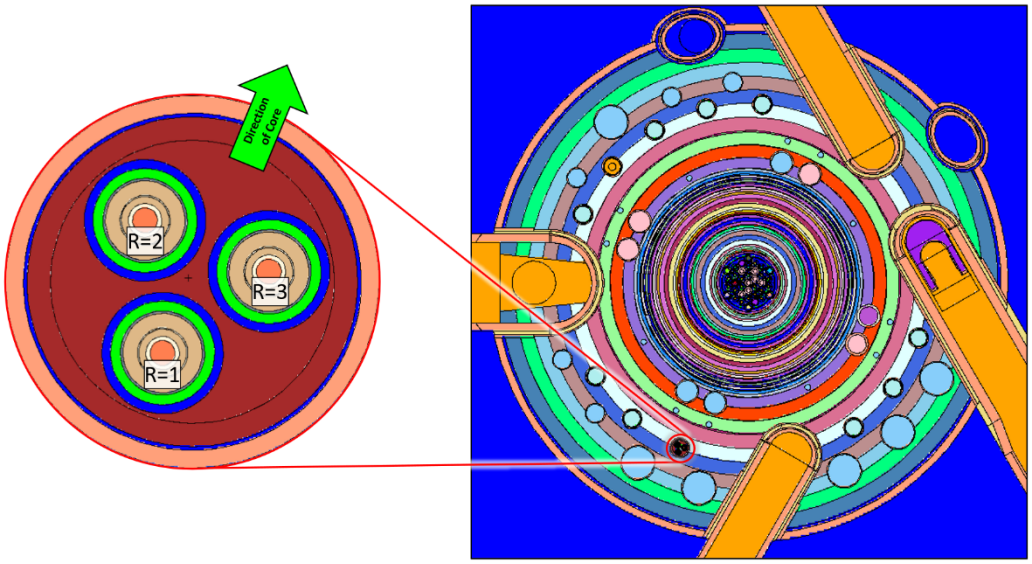

Figure 5. Top-down cross section of the neutronics model. Inset: Orientation and radial position designations of the targets.

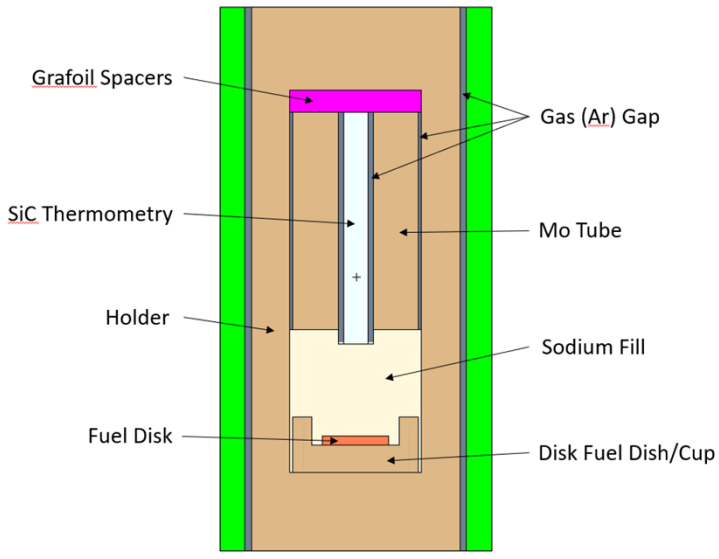

Figure 6. Neutronics model subcapsule geometry.

2.4 THERMAL ANALYSIS

All thermal analyses were evaluated using the Ansys finite element modeling software coupled with a custom, internally maintained set of APDL macros and a Python script. The macros are used to define material properties and to determine thermal conductance between components that are in contact with one another or that are separated by small gas gaps. The gaps are on the order of tens to hundreds of

microns. As a result, the heat transfer between the gaps is assumed to occur only by conduction and radiation. Gas gaps, which are also simulated to expand or contract due to thermal expansion of the components, is determined using temperature-dependent thermal expansion data, the temperatures of contact, and target surface nodes. The custom Python script is used to define material-dependent heat generation rates and fuel burnup values for specified irradiation times and target positions of the components by extracting the respective data from the neutronics output.

2.4.1 Boundary Conditions

The convective boundary conditions on the target's outer surface were 44.8 $kW \cdot m^{-2} \cdot K^{-1}$ convection heat transfer coefficient and 58°C bulk coolant temperature, as determined from previous RELAP5 calculations for an experiment with effectively identical flow conditions [11, 19].

2.4.2 Material Properties

The ORNL Irradiation Engineering Group (IEG) maintains a database of design and analysis calculations (DACs) that include temperature-dependent thermophysical material properties used in thermal analyses. The properties are obtained from a variety of literature sources, primarily CINDAS [20] and MatWeb [21]. The macro used to calculate gas mixture properties (for the mixture of helium and xenon from fission) is described in DAC-12-08-GAS_MIXTURE, Rev. 2 [22]. Helium is the fill gas in the initial subcapsule and target. The gas mixtures are combined based on the free volumes of the subcapsule as well as the total fuel volume and burnup. Component volumes are calculated in Ansys during the solution. Equations or values for sodium thermal conductivity, thermal expansion, Young's modulus, specific heat, and density were taken from Ref. [23]. Values for Poisson's ratio and microhardness were taken from Ref [24]. Table 1 displays the DACs used in this calculation, which are also available upon request.

Table 1. Experiment materials and material property references

Component	Material	Property Reference
Target housing, target end caps, springs	Stainless steel	DAC-10-16-PROP_SS304 [25]
Holder, end caps, tubes, dishes, thimbles	Molybdenum	DAC-10-11-PROP_MOLY [26]
Thermometry	SiC	DAC-10-06-PROP_SIC(IRR) [27]
Insulator disks	Grafoil	DAC-11-16-PROP_GRAFOIL [28]
Fuel disk	Uranium	DAC-11-09PROP_URANIUM [29]
Fill gas	Xenon	DAC-12-07-PROP_XENON [30]
	Helium	DAC-10-02-PROP_HELIUM [31]

2.5 EXPERIMENT TEST MATRIX

The original target temperatures for this experiment were selected to fill in a gap in the irradiation growth and swelling data for U metal in Mo-99 production-relevant temperature regimes (Section 1.1.); however, following preliminary scoping calculations, it was determined that temperatures below ~200°C would be impossible to achieve for all six fuel specimens of a single target, so the target temperatures were adjusted to those detailed in Table 2.

Table 2. Summary of planned irradiation conditions

Target ID	Number of irradiation cycles	Target temperature (°C)	Target fill gas (% He)	Irradiation location (R-A)	Target burnup (MWd/KgU)
Mini99-1	1	200	100	2-3	12–22
Mini99-2	1	400	100	3-3	12–22
Mini99-3	1	300	100	2-1	12–22

2.6 RESULTS OF ANALYSES

2.6.1 Neutronics Analysis Results

The calculated burnup and fission heat generation rates for a target at the RA:23 position are shown in Figure 7. In this target, subcapsule of RAS 231 is the closest to the axial midplane of the HFIR, and the fission heat generation rate and burnup are the highest, as expected. Additionally, there is an observed decrease in the fission heat generation rates near the midplane, which is a result of the burnup of initial U-235, lowering the fission rate over time. Further away from the axial midplane, this reduction is only observed for the first half of the cycle, and with a lower magnitude. Additionally, these positions (3–6) show an increase in heat generation rate near the end of cycle (EOC), which is due to an increasing flux magnitude caused by the control element adjustment. For these positions, fission heat generation is more sensitive to the change in flux at EOC than it is to the reduction of fission rate caused by fuel burnup.

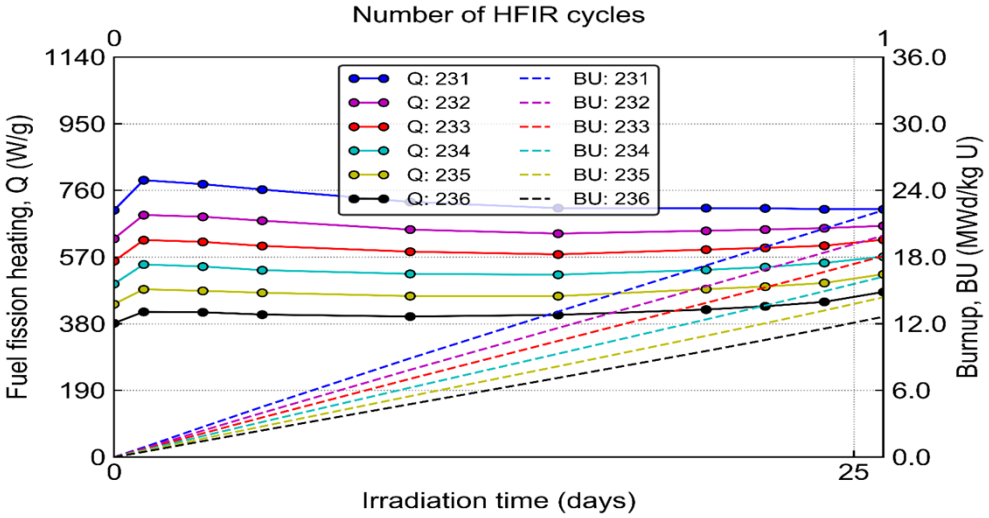

Figure 7. Predicted fission heat generation rates and burnups for Target Mini99-1 fuel.

The predicted burnup for all the specimens planned for irradiation are shown in Table 3. The burnup with respect to target position at R-A:2-1 is reversed relative to the other two targets. R-A:2-1 is below the HFIR midplane, whereas the other two are above the midplane, so R-A:2-1 is exposed to a mirrored flux profile. The burnup varies between roughly 12 to 22 MWd/kgU for all three targets.

Table 3. Burnup after one HFIR cycle (MWd/KgU)

Target ID	R-A	S1	S2	S3	S4	S5	S6
Mini99-1	2-3	22.2	19.9	18.1	16.2	14.4	12.6
Mini99-2	3-3	22.4	20.1	18.3	16.4	14.5	12.8
Mini99-3	2-1	12.3	13.7	15.5	17.4	19.2	21.0

2.6.2 Thermal Analysis Results

2.6.2.1 Ideal Case

The "ideal" case was analyzed using 0.4 mm thick fuel disk specimens and any holder outer diameter to achieve fuel temperatures closest to the target temperature of each target. Table 4 displays each subcapsule outer diameter (SubOD) used, the average fuel temperature for each subcapsule (Avg T), maximum and minimum temperatures witnessed over the 26 day cycle (Range), the average temperature of all fuel specimens of a target (T Avg), and the range of average temperatures among the six fuel specimens ("ΔT"). One notable detail of this data is for subcapsule 6 of Mini99-2, which does not reach its target fuel temperature of 400°C because the minimum holder diameter of 9 mm, established by the safety calculation of this experiment, had been reached.

Table 4. Ideal design thermal results across cycle

T_{Target} (°C)	Value[a,b,c]	Subcapsule Position						T_{Avg} (°C)[d]	ΔT (°C)[e]
		S1	S2	S3	S4	S5	S6		
Target ID Mini99-1 (RA: 2-3)									
200	SubOD (mm)	9.92	9.9	9.87	9.83	9.79	9.72	200.7	2.17
	Avg T (°C)	201.0	200.0	201.2	201.7	199.5	200.6		
	Range (°C)	10.9	8.4	8.7	12.6	16.4	20.6		
Target ID Mini99-2 (RA: 3-3)									
400	SubOD (mm)	9.4	9.33	9.23	9.11	9	9	398.3	46.6
	Avg T (°C)	403.8	406.2	409.6	409.2	397.9	363.1		
	Range (°C)	22.5	17.7	19.8	27.6	36.4	38.6		
Mini99- Target ID 3 (RA: 2-1)									
300	SubOD (mm)	9.32	9.45	9.54	9.61	9.66	9.7	300.1	2.29
	Avg T (°C)	300.9	301.0	300.5	300.0	299.6	298.7		
	Range (°C)	29.7	21.6	14.8	10.9	15.6	20.0		

[a] SubOD: Subcapsule outer diameter
[b] Avg T: Average fuel temperature for each subcapsule
[c] Range: Specimen's maximum and minimum temperature witnessed over the 26 day cycle
[d] T_{Avg} Average temperature of all fuel specimens of a target
[e] ΔT: The range of average temperatures among the six fuel specimens.

Figure 8 displays plots of the data for target Mini99-1 in comparison with a theoretical target with the same irradiation location and target geometry (same subcapsule ODs), but without sodium present. Figure 8a displays the average fuel temperature of all six subcapsules as a function of time through the cycle; Figure 8b displays the cycle averaged fuel temperature of each subcapsule position. The error bars in Figure 8a represent the range of fuel temperature over the six subcapsules; the error bars in Figure 8b represent the minimum and maxium in each subcapsule position's fuel temperature over a cycle.

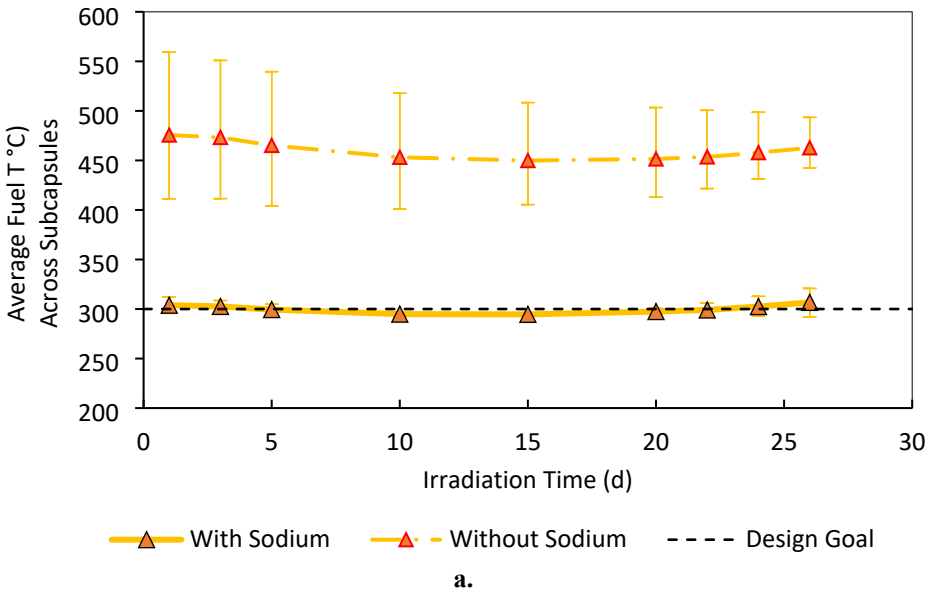

a.

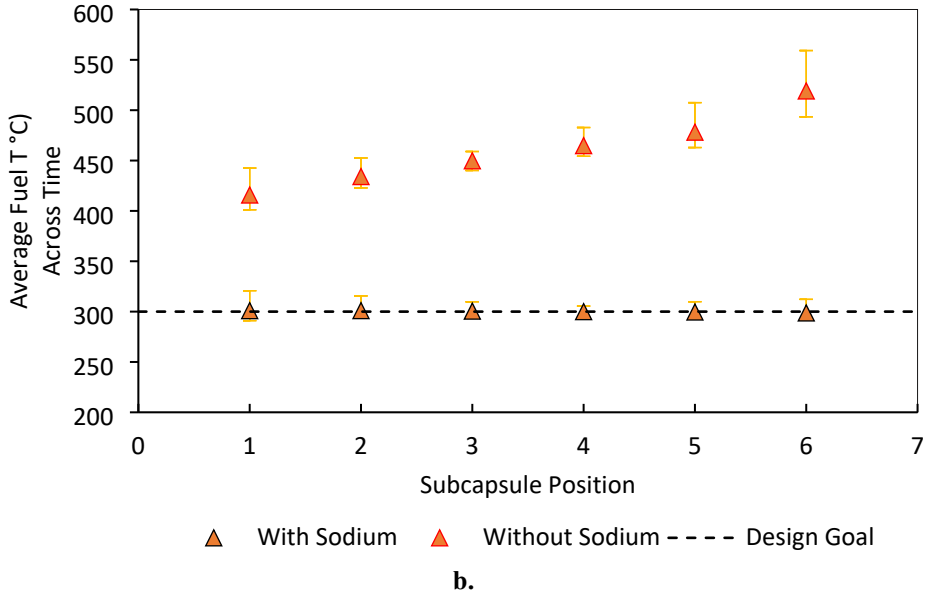

b.

Figure 8. Thermal results for Mini99-2 subcapsules with and without sodium. (a)Average fuel temperature of all six subcapsules across cycle. (b) Cycle-averaged fuel temperatures by subcapsule position.

2.6.2.2 Planned Design Case

The planned design case was analyzed because the fuel heights/thicknesses (DiskH) of the available fuel specimens were not exactly 0.4 mm and only certain holder diameters were available.

Table 5 displays the optimal target loading matrix (prioritizing Mini99-1) using the available fuel specimen thicknesses and holder ODs. This loading leads to an average fuel temperature per target within 25°C of the target temperature.

Table 5. Planned design thermal results across cycle

T_{Target} (°C)	Value[a,b,c,d]	Subcapsule position						T_{Avg} (°C)[e]	ΔT (°C)[f]
		S1	S2	S3	S4	S5	S6		
Target ID Mini99-1 (RA: 2-3)									
200	SubOD (mm)	9.92	9.87	9.83	9.76	9.83	9.66	196.1	19.6
	DiskH (mm)	0.375	0.369	0.341	0.287	0.385	0.283		
	Avg T (°C)	195.7	205.2	203.1	197.7	185.6	189.5		
	Range (°C)	10.1	8.0	9.3	13.3	15.0	20.1		
Target ID Mini99-2 (RA: 3-3)									
400	SubOD (mm)	9.32	9.33	9.15	9.06	9.06	9.06	391.8	66.4
	DiskH (mm)	0.366	0.375	0.363	0.367	0.369	0.385		
	Avg T (°C)	412.4	398.9	411.9	405.3	376.1	346.1		
	Range (°C)	20.6	16.4	19.8	27.1	34.1	36.5		
Mini99- Target ID 3 (RA: 2-1)									
300	SubOD (mm)	9.15	9.33	9.43	9.43	9.62	9.61	325.7	29.3
	DiskH (mm)	0.375	0.379	0.377	0.369	0.382	0.380		
	Avg T (°C)	327.4	324.7	325.6	340.8	311.5	324.2		
	Range (°C)	32.7	23.8	16.6	11.4	15.2	20.1		

[a] SubOD: Subcapsule outer diameter
[b] DiskH: Fuel Disk height/thickness
[c] Avg T: Average fuel temperature for each subcapsule
[d] Range: Specimen's maximum and minimum temperature witnessed over the 26 day cycle
[e] T_{Avg} Average temperature of all fuel specimens of a target
[f] ΔT: The range of average temperatures among the six fuel specimens.

2.6.2.3 Final As-Built Case

Six subcapsules were successfully welded, enough to fill a single target. (See Section 3.3.2.)

displays the expected thermal results for the single as-built target (Mini99-1), which was loaded to have two subcapsules with fuel temperatures of approximately 225°C and four subcapsules of approximately 300°C.

Table 6. Expected thermal results for as-built target

T_{Target} (°C)	Value[a,b,c,d]	Subcapsule position						T_{Avg} (°C)[e]	ΔT (°C)[f]
		S1	S2	S3	S4	S5	S6		
Target ID Mini99-1 (RA: 2-3)									
200	SubOD (mm)	9.86	9.82	9.61	9.43	9.31	9.15	271.2	92.4
	DiskH (mm)	0.367	0.363	0.382	0.377	0.287	0.283		
	Avg T (°C)	221.0	226.8	286.2	313.4	291.4	288.2		
	Range (°C)	10.9	8.5	14.0	22.1	27.1	32.8		

[a] SubOD: Subcapsule outer diameter
[b] DiskH: Fuel Disk height/thickness
[c] Avg T: Average fuel temperature for each subcapsule
[d] Range: Specimen's maximum and minimum temperature witnessed over the 26 day cycle
[e] T_{Avg} Average temperature of all fuel specimens of a target
[f] ΔT: The range of average temperatures among the six fuel specimens.

3. EXPERIMENT FABRICATION AND DELIVERY TO HFIR

3.1 FUEL SPECIMENS AND SODIUM-HANDLING REQUIREMENTS

The first challenge to fabricating the assemblies was due to the inclusion of the fuel specimens and sodium, which both have unique requirements for proper handling. Combining the two in a single experiment proved to be a logistical challenge that required careful planning and precise coordination between many ORNL facilities and resources. Many aspects of assembly, particularly the subcapsule assembly procedure detailed in Section 3.3.1, is justified due to these requirements.

The ORNL Nuclear Material Control and Accountability (NMC&A) group is responsible for the tracking of all nuclear material at ORNL. Each laboratory that handles nuclear material is designated a material balance area (MBA), and it keeps a running inventory of nuclear material in which the lab space manager (LSM) and the material balance area representative (MBAR) are responsible for maintaining. Nuclear material can be transferred between MBAs with the approval of transfer documentation signed by the receiving and outgoing MBARs and NMC&A staff and with the notification of the receiving/outgoing LSMs. A certified NMC&A material handler must be designated as the material's custodian during the transfer, and the material must be *in transit* when in non-MBA areas during transfer (No other activities may be performed when en route). To perform activities with a controlled material in a facility without an MBA, a project plan must be created and approved. The plan details the exact quantity and type of material to be moved, the activity that is to be performed, and a relatively short time period (on the order of days) in which the activity is to take place. In addition, two primary stipulations must be met when a project plan is used: (1) a certified NMC&A material handler must be always present with the material while it is out from the MBA, and (2) the material must be returned to the MBA of origination by 6 p.m. each day. This is relevant because the experiment required the creation and approval of two project plans to perform the assembly and welding.

One of the anticipated challenges of this experiment was the use and maintenance of elementally pure sodium within the subcapsules. Sodium oxidizes rapidly in air, producing sodium oxide (Na_2O) on the outer layer of exposed sodium. In addition to introducing unwanted oxide impurities to the experiment, which can cause the oxidation of housing and support components and increased difficulty during disassembly, sodium oxide is also less thermally conductive than elementally pure, liquid sodium. To mitigate the introduction and production of sodium oxide in the experiment, the assembly was performed in a glove box in Lab 24 of Building 4505, which maintained an environment with minimum oxygen levels, a capability not available in the lab in which the fuel material was stored. In addition, the integrity of the transport container used for transferring the assembled subcapsules and weld fixtures from the glove box in Lab 24 to the EB welder was not trusted to maintain an oxygen-free environment for extended periods. Only once the subcapsules were EB-welded and placed within a vacuum chamber, ensuring prevention of oxygen entering the subcapsules were the subcapsules able to be returned to the MBA for storage until ready for backfilling and seal welding. Therefore, two project plans had to be developed, the first including both the assembly and EB welding and the second including only the seal welding. As a result, not all subcapsules could be assembled and EB-welded within a single day, and the assembly of the subcapsules was performed in batches.

3.2 SECONDARY CONTAINMENT QUALIFICATION DEVELOPMENT

To ensure the safe and continued operation of the HFIR, ORNL maintains stringent safety and quality assurance (QA) requirements that must be met by all experiments. One of these requirements is proving the inability of an experiment to experience containment failure, which can result in coolant contamination and cause delays in scheduled irradiations. For standard experiments, only one

containment boundary is required. Safety calculations for these experiments, typically performed utilizing finite element analyses, must be provided that demonstrate the following items:

1. The targets can be exposed to
   a. a limiting condition scenario (LCS) at 130% reactor power and
   b. a 90% flow blockage scenario, with the target modeled at the reactor midplane and without exposing target containment components to temperatures exceeding their respective melting temperatures or pressures exceeding the maximum allowable pressure established in DAC-GEN-020977-A001 [32].
2. The internal components cannot cause the target containment to fail from axial or radial expansion.
3. The experiment is bounded by C-HFIR-2009-003 [33] in evaluating
   a. a scenario where two target channels are empty, which reduces flow in the remaining channel;
   b. a small break loss of cooling accident, and
   c. a loss of off-site power event.
4. Target containment will not melt due to a control cylinder ejection event.

Due to the presence of sodium in this experiment, which has a highly exothermic reaction with water, the subcapsules had to be qualified as secondary containment boundaries. Therefore, the same guidelines that applied to target containment components applied to the subcapsule containment components. This posed a particularly difficult challenge because there was no established bounding pressure for subcapsules as there is for the stainless-steel target housing (see item 1 above), and the molybdenum-to-molybdenum welds of the end caps to the holder are not ORNL safety–qualified welds. Therefore, a safety calculation defining internal and external pressure limits for MiniFuel subcapsules was developed following practices established by American Society of Mechanical Engineers Boiler and Pressure Vessel code Section VIII methodologies. The maximum subcapsule pressure calculated for LCS and 90% flow blockage scenarios was verified to be below the internal pressure limit, and the integrity of each subcapsule's weld was experimentally verified to prove the subcapsule's ability to withstand the maximum external pressure limit. Once welded and sealed, each subcapsule was subjected to the standard nondestructive examination (NDE) tests for MiniFuel subcapsules and were then exposed to pressures significantly beyond the established external pressure limit and retested. Passing this process demonstrated the ability of the subcapsules to withstand normal operating conditions of the HFIR, and allowed them to be accepted for use in the experiment.

3.3 SUBCAPSULE ASSEMBLY

3.3.1 Subcapsule Assembly Procedure

Prior to assembly, all subcapsule components were dimensionally inspected and cleaned according to HFIR-approved procedures, drawings, and sketches. They were then loaded into a glove box filled with N_2 to reduce the exposure of the specimens to oxygen and moisture. Figure 9 displays the layout of all individually labeled parts of a single subcapsule. (Sodium could not be labeled, and insulator disks were stored in bulk.).

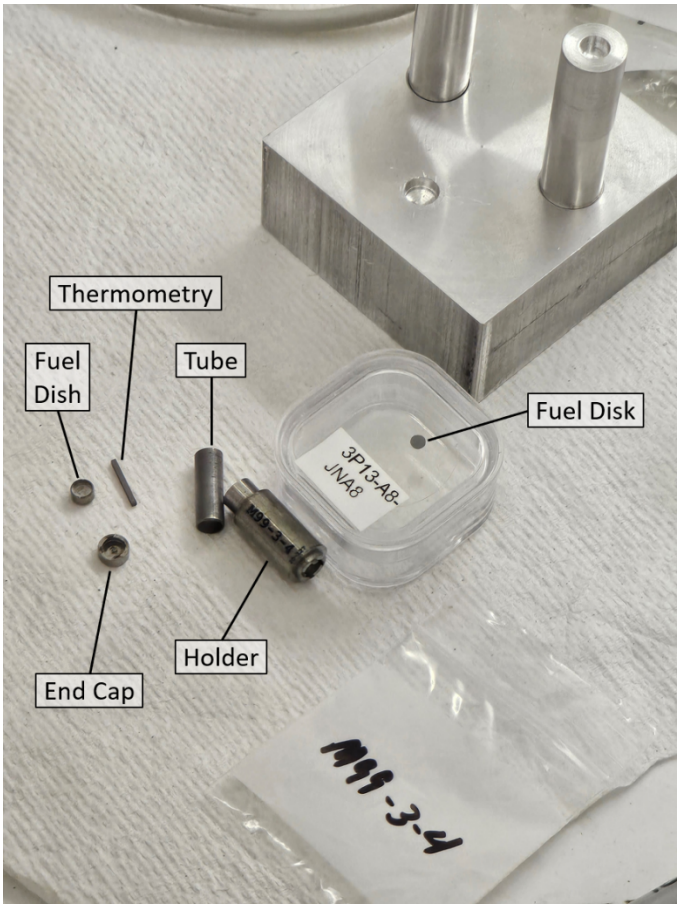

Figure 9. Subcapsule components in glove box. (Not pictured: sodium and insulator disks.)

The first step of the procedure was to place the fuel disk specimen into the fuel dish, followed by the molybdenum tube being placed on top, around the fuel dish. The tube was then flipped to have the bottom of the dish facing upward. The raw sodium, which had oxidized on the surface over time, was cut prior to each assembly to expose un-oxygenated sections. (See Figure 10a.) Pieces were extracted from this section, massed, and then placed on top of the upside-down tube and dish (Figure 10b). The holder was then placed over the sodium and tube, and the assembly was flipped back over. At that point the thermometry could be inserted into the top of the tube. The assemblies were then placed in a fixture that was heated to melt the sodium, allowing the tube and dish to properly seat within the holder (Figure 10c). The holder end caps could then be inserted into the holder. Each subcapsule assembly was then placed within the weld fixture, and the end caps were EB-welded to the holder. Figure 10d displays the weld fixtures containing welded subcapsules within the EB welding chamber.

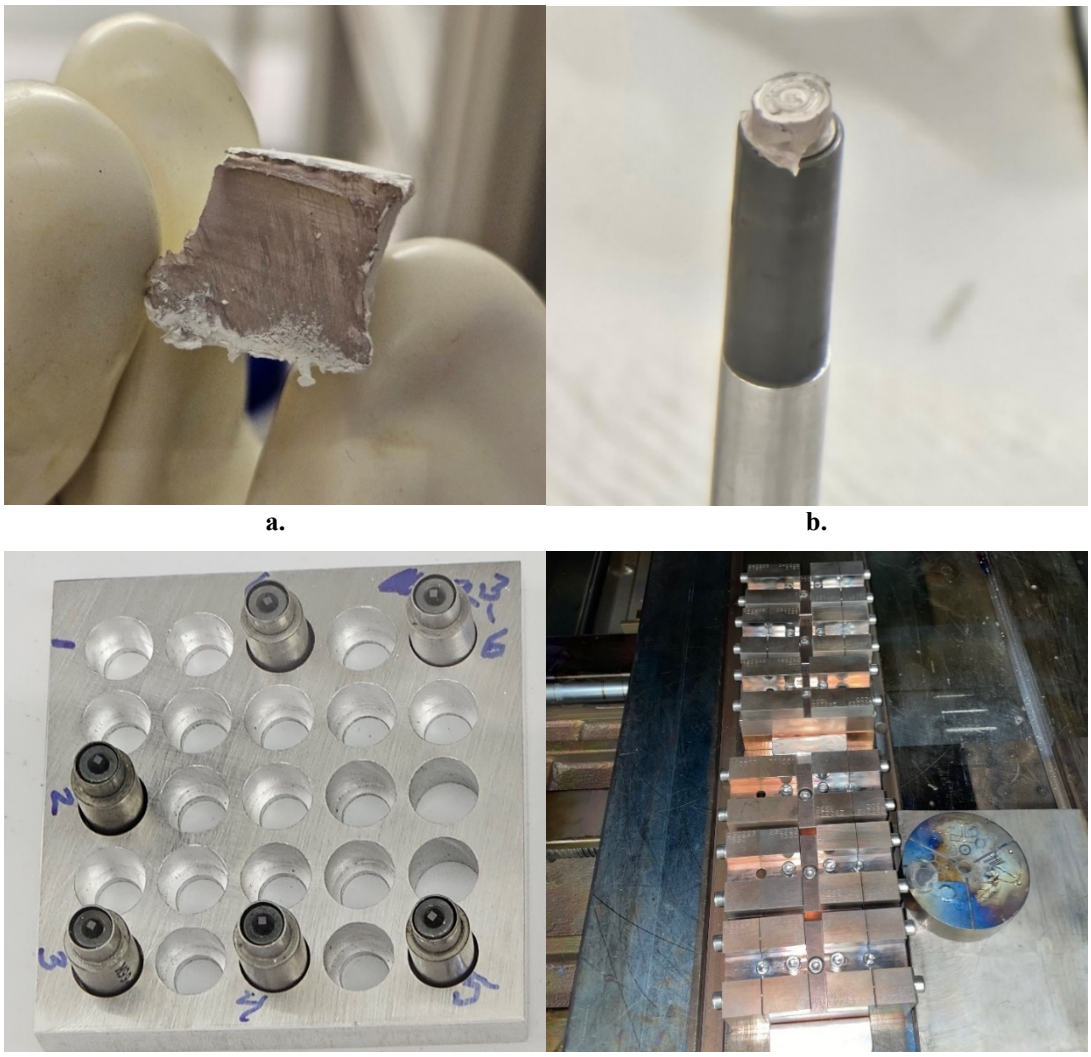

Figure 10. Subcapsule assembly pictures. (a) Cut raw sodium metal block. (b) Partially assembled subcapsule displaying sodium loading technique. (c) Subcapsules in holder tray used when melting sodium to seat internal components. (d) Subcapsules in weld fixture (heat sink) after EB welding.

The subcapsule assemblies were then placed inside a pressure vessel that was put under vacuum until it was placed inside a different glovebox, which was also evacuated and backfilled with ultrahigh-purity helium to atmospheric pressure. A small hole in each subcapsule end cap was seal-welded using a TIG welding procedure. The welds were visually inspected, and each subcapsule was sent for NDE. The NDEs for these subcapsules included an initial bubble test (using alcohol) and helium leak test, after which the subcapsules were pressurized with helium to 1,000 psi and reexamined with a final bubble and helium leak test. If the subcapsule passed the criteria of these tests, it was accepted for use.

3.3.2 Subcapsule Assembly Results

Six subcapsules were successfully fabricated for the experiment. Two target assembly campaigns were needed because welding issues were encountered during the first subcapsule fabrication. Welding of the molybdenum subcapsules was the greatest obstacle to fabrication. Therefore, a second target assembly campaign was undertaken to recover the fuel disks and to fabricate a second set of subcapsules.

During the first target assembly campaign, in 2022, only five of the eighteen subcapsules assemblies were successfully welded. Of the thirteen failed subcapsules, three had visibly failed the manual seal weld, and the remaining ten did not pass the helium leak test during NDE. The cause for these failures was theorized to be due to sodium migration up the internal holder wall and into the weld sites due to the heat deposited during the weld process. (Sodium was observed to have leaked out during a number of these welds.) To mitigate this phenomenon, a new weld fixture (Figure 10d) was designed and manufactured to house the subcapsules and act as a heat sink during the EB welding. In 2023, the thirteen failed subcapsules were disassembled, and the fuel specimens were recovered through chemical separation from the bonded sodium.

The second campaign took place in 2024. With five subcapsules successfully fabricated, only thirteen subcapsules were assembled in this campaign, reusing the fuel specimens recovered from the previous campaign's failed subcapsules. Unfortunately, only three of the subcapsules from the 2024 campaign were successfully welded. Due to the measures taken to ensure that the sodium did not migrate up the inner holder wall (meticulous assembly and handling of the subcapsules and use of the new heat sink), it was determined that sodium infiltration into the weld was likely not the primary source of failure, as previously theorized. In fact, the EB weld on each subcapsule was leak-tested (using a custom testing apparatus) prior to being seal-welded, which all passed; however, NDE results showed that most of the failed subcapsules leaked from the EB weld. Therefore, the current theory for the cause of weld failure is heat transfer from the TIG weld to the trepan weld.

Following the second assembly campaign, due to an already extremely extended fabrication time, it was decided to not attempt a third assembly campaign to remake enough subcapsules to fill three targets. Six of the eight successfully assembled and welded subcapsules were selected to construct a single irradiation target (Mini99-1). The target's expected fuel temperatures are detailed in Section 2.6.2.3.

3.4 TARGET ASSEMBLY

All target components were dimensionally inspected and cleaned according to HFIR-approved procedures, drawings, and sketches. **Error! Reference source not found.** displays the parts layout for the target assembly of Mini99-1. (Note: The target bottom end cap was welded onto the target housing prior to target assembly.)
After the subcapsules, centering thimbles, and compression springs were loaded, the target top end caps were welded to the target housings. The targets were then placed inside a pressure vessel that was put under vacuum until they were placed inside a glove box, which was also evacuated and backfilled with ultra-high-purity helium to a pressure equivalent to local atmospheric pressure. A small hole in each target assembly's top end cap was seal-welded using a TIG welding procedure. The welds were visually examined, and then the target was sent for NDE. The NDE tests included a helium leak test, hydrostatic compression at a pressure of 7.1 MPa (1,035 psi), mass comparisons before and after hydrostatic compression to ensure that no water penetrated the target assembly, another post-compression helium leak test, dye penetrant inspection, and radiographic inspection. The target passed all tests except the radiographic inspection; however, the cause of the failure was due to the backfill hole in the top end cap being considered a porosity in the target housing. A nonconformance report was written to confirm the housing and seal weld's integrity, which allowed the targets to be accepted.

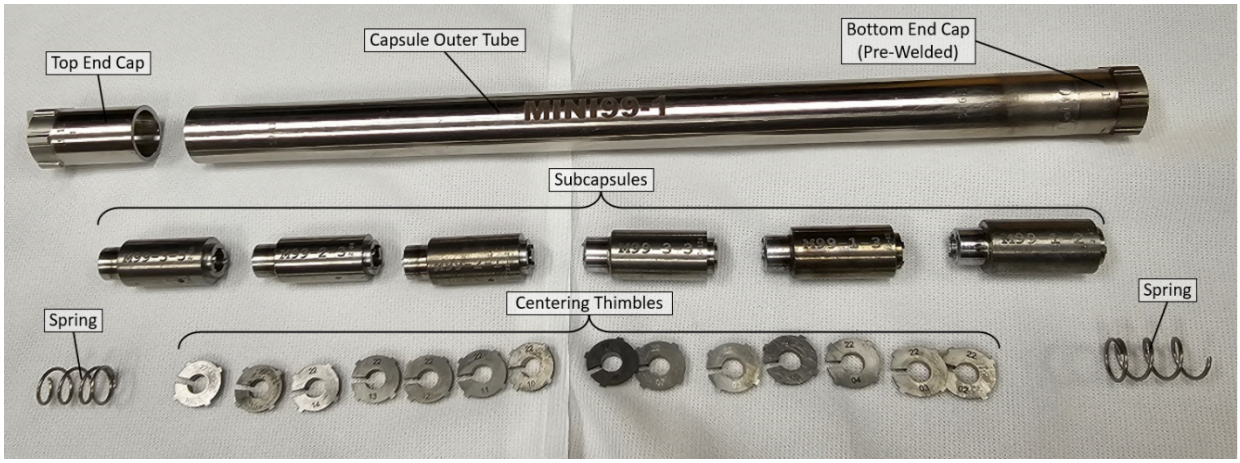

Figure 11. Parts layout of Mini99-1 target assembly.

Error! Reference source not found. displays Mini99-1's as-irradiated subcapsule details.

Table 7. Mini99-1 as-irradiated details

Subcapsule ID	RAS position	Fuel ID
M99-3-5	2-3-6	3P13-A8-JNAP
M99-2-3	2-3-5	3P13-A8-JNA4
M99-2-1	2-3-4	3P13-A8-JNAW
M99-3-3	2-3-3	3P13-A8-JNA9
M99-1-3	2-3-2	3P13-A8-JNAC
M99-1-2	2-3-1	3P13-A8-JNAY

3.5 FABRICATION PACKAGE AND DELIVERY TO HFIR

Each irradiation experiment requires a fabrication package that is reviewed by an independent design engineer, a lead QA representative, and a HFIR QA representative before it can be accepted for insertion into HFIR. The fabrication package must satisfy the requirements of the experiment authorization bases document (EABD). The irradiation of miniature fuel specimen experiments falls under EABD-HFIR-2018-001, Rev. 3 [34], which specifies requirements that the target must satisfy in the following areas:

- thermal safety analyses
- material certification
- dimensional inspection
- cleaning
- assembly procedure
- sample loading
- fill gas
- welding
- nondestructive examination

The fabrication packages for the Mini99-1 target was reviewed and approved by all parties and accepted by HFIR on March 22, 2024. The final signed acceptance page of the targets' EABD is provided in Appendix A. The experiment was inserted into HFIR's small VXF-11 position starting in cycle 506 (April 2024), which completed its full irradiation at 24.4 days.

4. FUTURE WORK

4.1 PIE PLAN

The irradiated Mini99-1 target will be shipped to ORNL's Irradiated Fuels Examination Laboratory for disassembly and PIE. The target will be cut open in-cell using a low-speed saw to recover the individual subcapsules. The two lower-temperature subcapsules (around 225°C target temperature) will be prioritized for subsequent PIE. The subcapsules will be cut open and disassembled to recover the fuel disk and the SiC thermometry. Laser flash analysis and profilometry measurements will be performed on the irradiated fuel disks to collect thermal diffusivity and swelling data, respectively. The SiC thermometry will be shipped to ORNL's Low-Activation Materials Development and Analysis Laboratory to be analyzed via dilatometry and to confirm the post-irradiation experiment irradiation temperature [35].

4.2 SUBCAPSULE WELD DEVELOPMENT

Molybdenum, specifically low-carbon arc-cast molybdenum, was selected as the primary material for structural components for several reasons. It has a high melting point (2,617°C), high strength, neutron transparency, and resistance to neutron swelling and chemical interactions; however, as detailed in Section 3.3.2, the welding of the subcapsules was the greatest challenge for this project. Mo/Mo welds involve a relatively exotic procedure on an industrial scale due to the inherent challenges, and studies for increasing its success rate are not well documented.

Some efforts have already been made at ORNL to improve the procedure, usually by leveraging data acquired from relevant experiments such as this one. For this experiment, the welding technology used (EB for trepan weld and manual TIG for seal weld), the input parameters associated with each weld technology (e.g., power, focus, and continuity), weld preparation (e.g., cleaning requirements, heat sink sensitivity), and spatial considerations (e.g., weld travel speed, weld joint size) were primarily determined from the results of previous MiniFuel experiments conducted at ORNL; however, the need for multiple assembly/welding campaigns and the prolonged experiment fabrication time allowed for some additional investigation. Between the two assembly campaigns, three dummy subcapsules were assembled, welded, then destructively examined (metallography of sections taken from the weld sites), an example of which can be seen in Figure 12.

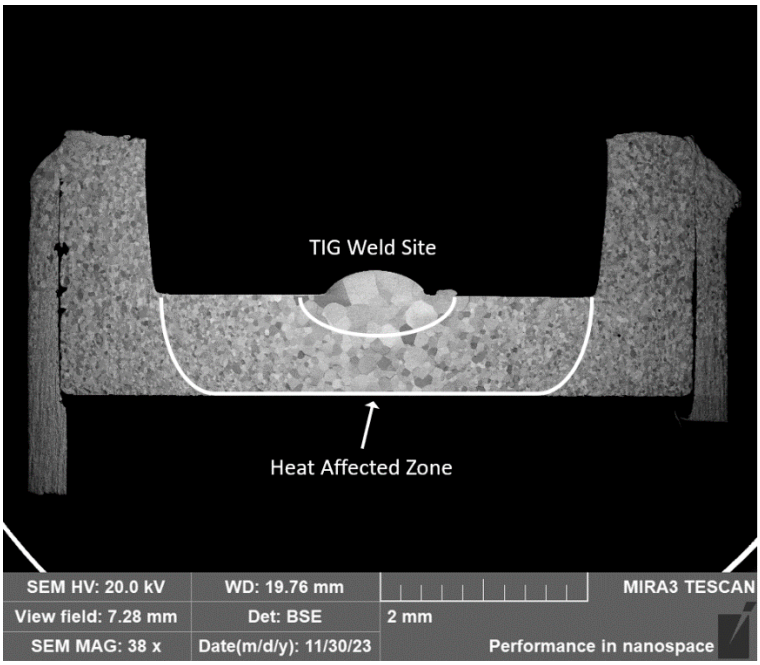

Figure 12. Metallography of subcapsule weld.

Scheduling difficulties for EB welding also prompted the investigation of laser welding for the trepan weld, which is still underway.

Automation of the TIG welding process is an obvious future capability that could improve the subcapsule welding procedure, but more drastic modifications to the experiment design may be required to produce consistent results. One proposed modification is to utilize end caps of a titanium alloy, likely Ti6Al4V, and to construct the subcapsule holder with a material transition from molybdenum to a similar Ti alloy at the weld site. Ti/Ti trepan welds are relatively well characterized. The lower melting temperature of Ti, in comparison with that of Mo, allows for improved weld penetration in the trepan weld and a lower power required for the TIG weld, which could mitigate the formation of cracks in the trepan weld due to heat transfer during the TIG weld. Of course, the use of Ti as containment material would require the design to be reevaluated to meet the safety requirements of the experiment (detailed in Section 3.2). Another design modification that has been proposed for future experiments is the placement of the backfill hole on the bottom of the holder rather than in the end cap. This would eliminate the possibility of heat dissipating from the TIG weld site out to the trepan weld, possibly disrupting its integrity; however, this design would not be viable for experiments with liquid metal present in the subcapsule.

4.3 FUTURE IRRADIATIONS

Currently, this campaign has no future irradiations planned; however, the option is available. Only six of the ~20 fuel specimens produced for this experiment have been irradiated, and the ability to successfully recover the specimens after sodium bonding and subcapsule assembly has been demonstrated (see Section 3.3.2). In addition, the use of sodium metal as a thermal conductor for high-temperature fuel experiments opens the door to a variety of experiment designs, particularly for high-burnup fuel investigations, which have previously been limited by fuel temperature.

5. SUMMARY AND CONCLUSIONS

The primary objectives of this experiment were to ascertain growth and swelling data for Mo-99 in production-relevant temperature regimes during irradiation of U-foil and to improve qualification capabilities for novel fuel concepts. This experiment established a novel MiniFuel experiment design for U specimen irradiation in HFIR, utilizing sodium bonding. Thermal analysis for this design shows that spatially and temporally isothermal fuel temperatures between 200°C and 400°C can be achieved. One MiniFuel target was successfully assembled and irradiated in the HFIR, providing proof of the sodium bonding capability and valuable data for two of the three target temperatures. This target also established the infrastructure for the qualification of experiments that require secondary containment and/or experiments containing molten metal, capabilities that were not available previously for HFIR experiments. The need for development of new technical areas of the MiniFuel design and assembly procedure have been identified, and the planned PIE for the target will validate the analysis and sodium bonding capability.

WORKS CITED

[1] National Academies of Sciences, Engineering, and Medicine, Molybdenum-99 for Medical Imaging, Washington, DC: The National Academies Press., 2016.

[2] National Nuclear Security Administration, "NNSA helps global health industry achieve major nuclear nonproliferation milestone," 28 March 2023. [Online]. Available: https://www.energy.gov/nnsa/articles/nnsa-helps-global-health-industry-achieve-major-nuclear-nonproliferation-milestone.

[3] B. Hudson, K. Westmacott and M. Makin, "Dislocation loops and irradiation growth in alpha uranium," *Philisophical Magazine 7(75),* pp. 377-392, 1962.

[4] J. H. Kittel and S. H. Paine, "Effect of irradiation on fuel materials," Argonne National Lab, Lemont, IL, 1958.

[5] J. H. Kittel and J. H. Paine, "Effects of High Burnup on Natural Uranium," *Nuclear Science and Engineering,* vol. 3, no. 3, pp. 250-268, 1957.

[6] S. G. Pugh, "Damage Occurring in Uranium during Burn-up," in *International Conference on the Peaceful Uses of Atomic Energy, Volume 7: Nuclear Chemistry and Effects of Irradiation (*, 1956.

[7] A. C. Roberts and A. H. Cottrell, "XXII. Creep of alpha uranium during irradiation with neutrons," *Philosophical Magazine 1.8,* pp. 711-717, 1956.

[8] G. W. Greenwood, A. J. E. Foreman and D. E. Rimmer, "The role of vacancies and dislocations in the nucleation and growth of gas bubbles in irradiated fissile material," *Journal of Nuclear Materials,* vol. 1, no. 4, pp. 305-324, 1959.

[9] R. D. Leggett, B. Mastel and T. K. Bierlein, "Irradiation Behavior of High Purity Uranium, Reprot HW-79559," 1963.

[10] S. F. Pugh, "Swelling in alpha uranium due to irradiation," *Journal of Nuclear Materials,* vol. 4, no. 2, pp. 177-199, 1961.

[11] C. M. Petrie, "Separate effects irradiation testing of miniature fuel specimens," *Journal of Nuclear Materials,* vol. 526, 2019.

[12] R. Cheverton and T. Sims, "ORNL-4621, HFIR Core Nuclear Design," Oak Ridge National Laboratory, Oak Ridge, TN, 1971.

[13] R. C. Gallagher, "ORNL/TM-2020/1658; Analysis and Design of High-Power TRISO Fuel Compact Irradiation in HFIR," Oak Ridge National Laboratory, 2021.

[14] J. P. Gorton, Z. G. Wallen and C. M. Petrie, "Modifications to MiniFuel Vehicle to Enable Higher Temperature UO2 Irradiation Capabilities, ORNL/SPR-2021/2096," Oak Ridge National Laboratory, 2021.

[15] "High Flux Isotope Reactor Technical Parameters," Oak Ridge National Laboratory, [Online]. Available: https://neutrons.ornl.gov/hfir/parameters.

[16] S. C. Wilson, S. M. Mosher, C. R. Daily and D. Chandler, "ORNL/TM-2020/1742; HFIRCON Version 1.0.5 User Guide," Oak Ridge National Laboratory, 2020.

[17] G. Ilas, D. Chandler, B. J. Ade, E. E. Sunny, B. R. Betzler and D. Pinkston, "Modeling and Simulations for the High Flux Isotope Reactor Cycle 400. ORNL/TM-2015/36," Oak Ridge National Laboratory, 2015.

[18] J. Burns, "Heat Generation Rates of Small-Scale Ceramic Fuel Samples and Structural Components in an lrradiation Experiment in an lnner Small VXF Position in HFIR, C-HFIR-2017-040," Oak Ridge National Laboratory, 2018.

[19] L. Ott, G. Bell, R. Ellis, J. McDuffee and R. Morris, "Irradiation of SiC clad fuel in the HFIR," in *Proceedings of Top Fuel 2013*, Charlotte, NC, 2013.

[20] "CINDAS, LLC: global benchmark for critically evaluated materials properties," CINDAS, LLC, [Online]. Available: http://cindasdata.com..
[21] M. LLC, "Material property data," MatWeb, [Online]. Available: http://www.matweb.com. [Accessed 2020].
[22] J. L. McDuffee, "DAC-12-08-GAS MIXTURE, Rev. 2, Thermophysical Property Calculator for Arbitrary Mixtures of Monotomic Gases," Oak Ridge National Laboratory, 2015.
[23] O. J. Foust, SODIUM-NaK ENGINEERING HANDBOOK. VOLUME I. SODIUM CHEMISTRY AND PHYSICAL PROPERTIES., Gordon and Breach, 1972.
[24] F. Cardarelli, Materials Handbook: A Concise Desktop Reference, 3rd Edition ed., Springer, 2018.
[25] J. L. McDuffee, *Thermophysical Properties for 304 Stainless Steel. DAC-10-16-PROP_SS304, Rev.1,* Oak Ridge National Laboratory, 2013.
[26] J. L. McDuffee, *Thermophysical Properties for Molybdenum. DAC-10-11-PROP_MOLY, Rev. 1,* 2013.
[27] J. L. McDuffee, *Thermophysical Properties for Irradiated Silicon Carbide. DAC-10-06-PROP_SIC(IRR), Rev. 3.,* Oak Ridge National Laboratory, 2013.
[28] J. L. McDuffee, *Thermophysical Properties for Flexible Graphite. DAC-11-16-PROP_GRAFOIL, Rev.0,* Oak Ridge National Laboratory, 2013.
[29] J. L. McDuffee, *Thermophysical Properties for Uranium Metal. DAC-11-08-PROP_URANIUM,* Oak Ridge National Laboratory, 2013.
[30] J. L. McDuffee, *Thermophysical Properties for Xenon. DAC-12-07-PROP_XENON, Rev.0,* Oak Ridge National Laboratory, 2012.
[31] J. L. McDuffee, *Thermophysical Properties for Helium. DAC-10-02-PROP_HELIUM, Rev. 0,* 2010.
[32] M. Lower, "DAC-GEN-020977-A001: VXK Experiment ASME Code Calculations," Oak Ridge National Laboratory, 2010.
[33] J. McDuffee, "C-HFIR-2009-003 Rev. 0: RELAP5 Transient Analysis for a VXF Fuel Irradiation Facility," Oak Rideg National Laboratory, Oak Ridge Tennessee, 2010.
[34] M. Fuller, *Irradiation of Miniature Fuel Specimens in the Inner Small VXF Positions. EABD-HFIR-2018-001, Rev.3,* Oak Ridge National Laboratory, 2024.
[35] A. A. Campbell, W. D. Porter, Y. Katoh and L. L. Snead, "Method for analyzing passive silicon carbide thermometry with a continuous dilatometer to determine irradiation temperature," *Nuclear Instruments and Methods in Physics Research Section B: Beam Interactions with Materials and Atoms,* vol. 370, no. 0168-583X, pp. 49-58, 2016.

APPENDIX A. EXPERIMENT AUTHORIZATION BASES DOCUMENT

Experiment Authorization Bases Document: EABD-HFIR-2018-001 Title: "Irradiation of Miniature Fuel Specimens in the Inner Small VXF Positions" Prepared By: Michael Fuller Date:1/10/2024	**Rev 3** Page 10 of 14

Section 6: Acceptance for Use of As-Built Experiment Capsule

Note: This section is used to document acceptance of the as-built experiment for reactor installation and irradiation. This section is completed **after** completion of Section 2. See notes for explanation of signatures.

1. List Applicable Component Identifications:

Basket ID: Mini99-1 in MFB
Flux monitor IDs for Basket:

Target I.D. (as marked)	Dummy target
Mini99-1	☐
	☐
	☐
	☐
	☐
	☐
	☐
	☐
	☐

2. Approvals (see notes for explanation of signature responsibilities)

Zane Wallen/Richard Howard Lead Experimenter	Zane G. Wallen Digitally signed by Zane G. Wallen Date: 2024.03.21 10:11:52 -04'00' Richard Howard Digitally signed by Richard Howard Date: 2024.03.21 10:36:00 -04'00' Lead Experimenter (signature)		Date
Steven DeFalco Lead QA	Steven DeFalco Digitally signed by Steven DeFalco Date: 2024.03.21 10:48:40 -04'00' Lead QA (signature)		Date
Andrew Ross RRD NQR	Andrew Ross Digitally signed by Andrew Ross Date: 2024.03.21 14:40:53 -04'00' RRD QA (signature)		Date
Michael Fuller E&FI Staff	Michael Fuller Digitally signed by Michael Fuller Date: 2024.03.21 15:49:16 -04'00' E&FI Staff (signature)	BLL	Date
* B. L. Lee RRD Criticality Safety Officer	Billy Lee Jr Digitally signed by Billy Lee Jr Date: 2024.03.20 07:55:56 -04'00' RRD Criticality Safety Officer (signature)	3/22/24	Date
David Stanley HFIR MBA Representative	David C. Stanley Digitally signed by David C. Stanley Date: 2024.03.22 11:43:17 -04'00' HFIR MBA Representative (signature)		Date
David Stanley HFIR Operations (print name)	David C. Stanley Digitally signed by David C. Stanley Date: 2024.03.22 11:43:37 -04'00' HFIR Operations (signature)		Date

* RRD Criticality Safety Office item is pre-signed on the basis that the design content will not deviate and conforms to the specifications contained in this EABD. If Att B identifies a NCR or Deviation then the CSO shall be included as party to the specific document or shall acknowledge the change by initial and date in the above signature block.